Cellular/Molecular

Effects of NALCN-Encoded Na$^+$ Leak Currents on the Repetitive Firing Properties of SCN Neurons Depend on K$^+$-Driven Rhythmic Changes in Input Resistance

Nien-Du Yang,[1] Rebecca L. Mellor,[2] Tracey O. Hermanstyne,[3] and Jeanne M. Nerbonne[1,2,3]

[1]Department of Biomedical Engineering, Washington University, St. Louis, Missouri 63110, [2]Department of Medicine, Cardiovascular Division, and [3]Department of Developmental Biology, Washington University School of Medicine, St. Louis, Missouri 63110

Neurons in the suprachiasmatic nucleus (SCN) generate circadian changes in the rates of spontaneous action potential firing that regulate and synchronize daily rhythms in physiology and behavior. Considerable evidence suggests that daily rhythms in the repetitive firing rates (higher during the day than at night) of SCN neurons are mediated by changes in subthreshold potassium (K$^+$) conductance(s). An alternative "bicycle" model for circadian regulation of membrane excitability in clock neurons, however, suggests that an increase in NALCN-encoded sodium (Na$^+$) leak conductance underlies daytime increases in firing rates. The experiments reported here explored the role of Na$^+$ leak currents in regulating daytime and nighttime repetitive firing rates in identified adult male and female mouse SCN neurons: vasoactive intestinal peptide-expressing (VIP$^+$), neuromedin S-expressing (NMS$^+$) and gastrin-releasing peptide-expressing (GRP$^+$) cells. Whole-cell recordings from VIP$^+$, NMS$^+$, and GRP$^+$ neurons in acute SCN slices revealed that Na$^+$ leak current amplitudes/densities are similar during the day and at night, but have a larger impact on membrane potentials in daytime neurons. Additional experiments, using an *in vivo* conditional knockout approach, demonstrated that NALCN-encoded Na$^+$ currents selectively regulate daytime repetitive firing rates of adult SCN neurons. Dynamic clamp-mediated manipulation revealed that the effects of NALCN-encoded Na$^+$ currents on the repetitive firing rates of SCN neurons depend on K$^+$ current-driven changes in input resistances. Together, these findings demonstrate that NALCN-encoded Na$^+$ leak channels contribute to regulating daily rhythms in the excitability of SCN neurons by a mechanism that depends on K$^+$ current-mediated rhythmic changes in intrinsic membrane properties.

Key words: circadian rhythms; NALCN channel; neuronal excitability; SCN

Significance Statement

Elucidating the ionic mechanisms responsible for generating daily rhythms in the rates of spontaneous action potential firing of neurons in the suprachiasmatic nucleus (SCN), the master circadian pacemaker in mammals, is an important step toward understanding how the molecular clock controls circadian rhythms in physiology and behavior. While numerous studies have focused on identifying subthreshold K$^+$ channel(s) that mediate day-night changes in the firing rates of SCN neurons, a role for Na$^+$ leak currents has also been suggested. The results of the experiments presented here demonstrate that NALCN-encoded Na$^+$ leak currents differentially modulate daily rhythms in the daytime/nighttime repetitive firing rates of SCN neurons as a consequence of rhythmic changes in subthreshold K$^+$ currents.

Introduction

In mammals, the suprachiasmatic nucleus (SCN), a small bilateral nucleus in the hypothalamus, is the central circadian clock that coordinates daily rhythms in physiology and behavior (Colwell, 2011; Herzog et al., 2017; Hastings et al., 2018, 2019). Neurons in the SCN display cell-autonomous, rhythmic spontaneous repetitive action potential firing at rates that are higher during the day than at night (Inouye and Kawamura, 1979; Green and Gillette, 1982; Welsh et al., 1995). Although the critical ionic conductance(s) driving these rhythms have not been defined, electrophysiological studies have shown that the daily oscillations in the repetitive firing rates of SCN neurons are linked to changes in input resistances and membrane

potentials (Jiang et al., 1997; de Jeu et al., 1998; Pennartz et al., 2002), driven by rhythmic changes in the functional expression of subthreshold potassium (K$^+$) currents (Kuhlman and McMahon, 2004, 2006; Allen et al., 2017; Harvey et al., 2020). The higher repetitive firing rates of daytime SCN neurons are associated with increased input resistances and more depolarized membrane potentials, resulting from a decrease in subthreshold K$^+$ conductance(s). The lower repetitive firing rates of nighttime SCN neurons, in contrast, are associated with decreased input resistances and hyperpolarized membrane potentials, mediated by increased subthreshold K$^+$ conductance(s).

Multiple types of K$^+$ currents have been identified in SCN neurons and shown to play important roles in shaping action potentials and regulating repetitive firing (Itri et al., 2005, 2010; Meredith et al., 2006; Pitts et al., 2006; Kent and Meredith, 2008; Kudo et al., 2011; Granados-Fuentes et al., 2012, 2015; Whitt et al., 2016; Hermanstyne et al., 2017; Harvey et al., 2020), and recently a critical role for Kv12-encoded K$^+$ channels in driving the day-night switch in repetitive firing rates of SCN neurons was revealed (Hermanstyne et al., 2023).

An alternative, "bicycle" model for the circadian regulation of membrane excitability in posterior dorsal neurons 1 (DN1p) that underlie the molecular clock in *Drosophila*, however, has also been proposed (Flourakis et al., 2015) and suggested to be conserved in mammalian SCN neurons. In this model, a daytime increase in a TTX-insensitive sodium (Na$^+$) leak current, encoded by the *narrow abdomen (na)* locus, drives the daytime depolarization and increase in the rate of spontaneous action potential firing of DN1p neurons, and an increase in K$^+$ current(s) underlies the nighttime hyperpolarization and reduction in firing rates (Flourakis et al., 2015). Additional experiments revealed that forebrain-specific knockout (KO) of *Nalcn*, the mouse ortholog of *na*, hyperpolarized the membrane potentials and eliminated spontaneous firing in postnatal day 17-21 SCN neurons (Flourakis et al., 2015). The targeted deletion of *Nalcn* in forebrain neurons, however, also resulted in premature death (around postnatal day 21), precluding determination of the critical developmental role(s) of *Nalcn* and/or delineation of the functional role of NALCN-encoded Na$^+$ leak currents in adult SCN neurons.

Combining cellular electrophysiological, pharmacological, *in vivo* molecular genetic, and computational approaches, the experiments here were designed to determine directly the role(s) of Na$^+$ leak currents in mediating day-night rhythms in the repetitive firing rates and intrinsic membrane properties of adult SCN neurons. In addition, because it is well documented that there is considerable cellular heterogeneity in the SCN with neurons expressing different neuropeptides, such as vasoactive intestinal peptide (VIP), arginine vasopressin (AVP), neuromedin S (NMS), and gastrin-releasing peptide (GRP) (Abrahamson and Moore, 2001; Hastings et al., 2018, 2019; Wen et al., 2020), and electrophysiological properties (de Jeu et al., 1998; Pennartz et al., 1998; Kononenko and Dudek, 2004; Hermanstyne et al., 2016; Mazuski et al., 2018; Collins et al., 2020; Patton et al., 2020; Hermanstyne et al., 2023), experiments were conducted on identified, VIP-, NMS-, and GRP-expressing SCN neurons. The results presented suggest a molecular mechanism in which the impact of NALCN-encoded Na$^+$ leak currents on the repetitive firing rates of mature SCN neurons depends directly on daily rhythms in the functional expression of subthreshold K$^+$ currents.

Materials and Methods

Animals. The mice used in this study were as follows: (1) WT (C57BL/6J, stock #JAX 000664, The Jackson Laboratory); (2) VIP-EGFP (stock #031009-UCD, 37Gsat, Mutant Mouse Resource and Research Center); (3) NMS-iCre (stock #JAX 027205, The Jackson Laboratory) (Lee et al., 2015); (4) GRP-Cre (obtained from Zhou-Feng Chen at Washington University); (5) Ai9 (Rosa-CAG-LSL-tdTomato-WPRE, stock #JAX 007909, The Jackson Laboratory) (Madisen et al., 2010); and, (6) *Nalcn*$^{fl/fl}$ (obtained from Dejian Ren at University of Pennsylvania) (Flourakis et al., 2015). The VIP-EGFP line was generated by backcrossing the VIP-EGFP mice obtained in the CD1 background to C57BL/6J for 10 generations. All other lines were acquired in C57BL/6J background. The NMS-tdTomato and GRP-tdTomato mouse lines were generated by crossing NMS-iCre or GRP-Cre mice, respectively, with Ai9 reporter mice (Madisen et al., 2010; Lee et al., 2015; Yu et al., 2017). Mice were housed in one of the animal facilities at Washington University Medical School in a controlled environment with an ambient temperature of 23°C and humidity of 50 ± 10% under either a standard (lights on at 7:00 A.M. and off at 7:00 P.M.) or a reversed (lights off at 7:00 A.M. and on at 7:00 P.M.) 12/12 h light/dark (LD) cycle with food and water available *ad libitum*. Zeitgeber times (ZTs) are indicated throughout with ZT0 and ZT12 corresponding to the time of "lights on" and "lights off," respectively, in the animal facility. All animal procedures were performed in accordance with the protocol (#20-2253) approved by the Washington University Institutional Animal Care and Use Committee and conformed to the United States National Institutes of Health Guidelines for the Care and Use of Laboratory Animals.

Stereotaxic virus injections and conditional KO of Nalcn. Virus injections were performed on 6-week-old WT and *Nalcn*$^{fl/fl}$ male and female mice under sterile conditions using previously described procedures (Hermanstyne et al., 2017). Briefly, each mouse was anesthetized with a ketamine/xylazine mixture (86 mg·kg^{-1}/13 mg·kg^{-1}, i.p.), and the head was then secured in a stereotaxic frame (Kopf Instruments). After shaving the head, Betadine was applied to cleanse and sterilize the shaved region, and the skull was exposed via a small incision along the midline. For conditional KO of *Nalcn*, bilateral injections (600 nl each) of an adeno-associated virus (AAV) serotype 5 encoding Cre recombinase and dTomato (AAV5-hSyn-Cre-P2A-dTomato, titer ≥7×10^{12} vg/ml, #107738-AAV5, Addgene) were made into the SCN of *Nalcn*$^{fl/fl}$ mice (injection coordinates relative to bregma were as follows: AP −0.32 mm, ML ±0.1 mm, DV −5.6 mm) using glass pipettes (15-25 μm tip diameter) connected to a Nanoject II Auto-Nanoliter Injector (Drummond Scientific). Similar bilateral virus injections were made into the SCN of WT mice (to serve as controls). After injections were completed, pipettes were left in place for ~5 min before being retracted to minimize solution reflux during pipette withdrawal. Gel control super glue (Loctite) was used to close the incision. Postsurgery analgesia was provided by subcutaneous injection of buprenorphine sustained-release (Bup SR-LAB, 0.05 ml of 1 mg/ml, Zoopharm).

Acute SCN slice preparation. Acute SCN slices were prepared from adult male and female mice (8-12 weeks) maintained in either a standard or a reversed LD cycle (Hermanstyne et al., 2016, 2017). "Daytime" slices were routinely prepared at ZT4 from mice maintained in the standard LD cycle, and "nighttime" slices were prepared at ZT16 from mice maintained in the reversed LD cycle for at least 2 weeks. For the preparation of "daytime" slices, mice were transported to the laboratory and anesthetized with 1.25% Avertin (2,2,2-tribromoethanol and tert-amyl alcohol in 0.9% NaCl; 0.025 ml/g body weight; Acros Organics), followed by transcardial perfusion with ice-cold slicing solution (240 mM sucrose, 2.5 mM KCl, 1.25 mM NaH$_2$PO$_4$, 25 mM NaHCO$_3$, 0.5 mM CaCl$_2$, 7 mM MgCl$_2$, oxygenated with 95% O$_2$ and 5% CO$_2$). Brains were then quickly removed, placed in oxygenated ice-cold slicing solution, and 300 μm coronal slices were cut on a Leica VT1000 S vibrating blade microtome (Leica Microsystems). Slices containing the bilateral SCN (typically 2 slices per mouse) were subsequently incubated at room temperature (23°C-25°C) in a holding chamber with ACSF (125 mM NaCl, 2.5 mM KCl, 1.25 mM NaH$_2$PO$_4$, 25 mM NaHCO$_3$, 2 mM CaCl$_2$, 1 mM MgCl$_2$, 25 mM glucose, ~310 mOsm, oxygenated with 95% O$_2$ and 5% CO$_2$) for at least
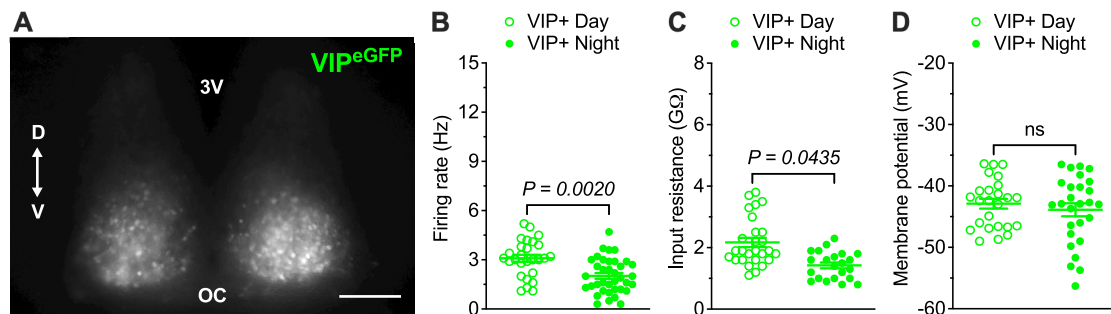
Figure 1. VIP⁺ SCN neurons exhibit day-night differences in spontaneous repetitive firing rates and input resistances. ***A***, Fluorescence image of a representative SCN slice prepared from an adult VIP-EGFP mouse. Scale bar, 100 μm. V, Ventral; D, dorsal; 3V, third ventricle; OC, optic chiasm. The spontaneous firing rates (***B***), input resistances (***C***), and membrane potentials (***D***) of individual VIP⁺ SCN neurons, measured in slices prepared during the day (open circles, $n = 25$-27) or at night (filled circles, $n = 22$-37) are plotted. Data are mean $\pm$ SEM; p values are also indicated.

1 h before being used for recording. To prepare "nighttime" slices, mice maintained in the reversed LD cycle were removed from their cages in the animal facility under red (~630 nm) light, transported to the laboratory in light-tight boxes, anesthetized with 1.25% Avertin, perfused with ice-cold slicing solutions, and brains were removed under red light. Slices were then cut as described above for daytime slices.

Electrophysiological recordings. Electrophysiological recordings were obtained at room temperature during the day (ZT5-ZT11) or at night (ZT17-ZT23) from SCN neurons in acute slices prepared from mice maintained in the standard or reversed LD cycle. SCN neurons were visually identified using a Nikon Eclipse E600FN upright microscope equipped with differential interference contrast optics with infrared illumination. SCN neurons expressing fluorescent proteins were identified with a Nikon 96320 F/EGFP or a Nikon 49008 ET mCH/TR fluorescence filter cube. Images were captured with a Moment CMOS camera (Teledyne Photometrics) and MetaMorph acquisition software (Molecular Devices). Slices were continuously perfused with oxygenated ACSF. Pipettes were fabricated from standard wall borosilicate glass (G150F-4, #64-0793, Warner Instruments) with a Sutter P-87 micropipette puller (Sutter Instrument). Current-clamp and voltage-clamp recordings were obtained with pipettes (with resistances of 4-7 Mohms) filled with the standard internal solution containing the following:144 mM K-gluconate, 10 mM HEPES. 3 mM MgCl₂, 4 mM Mg-ATP, 0.5 mM Na-GTP, 0.2 mM EGTA (~300 mOsm, pH 7.3). Data were acquired using a Multiclamp 700B amplifier (Molecular Devices) interfaced to a Dell personal computer with a Digidata 1550B and the pCLAMP 11 software (Molecular Devices). Signals were low-pass-filtered at 10 kHz and sampled at 20 kHz. In all recordings, tip potentials were zeroed before forming pipette-membrane seals.

For each cell, spontaneous action potential firing activity was first monitored during loose-patch cell-attached recording for ~1 min. This was done routinely before establishing the whole-cell recording configuration. Following the formation of a Gohm seal, the whole-cell configuration was established, and whole-cell membrane capacitances and series resistances were compensated. Whole-cell spontaneous firing activity was then recorded for ~1 min and compared with the data acquired in the cell-attached mode. If any differences in the frequency and/or pattern of repetitive firing in the cell-attached and whole-cell recording configurations were evident, recordings were terminated and any data acquired from these cells were not included in the analyses. To measure cell input resistance in current-clamp mode, a hyperpolarizing holding current was first introduced to maintain the membrane potential at ~−70 mV and to silence firing, and small (±5 pA) 300 ms currents were injected. For voltage-clamp recordings, membrane capacitances and series resistances were compensated electronically. Series resistances were in the range of 15-25 Mohms, and were routinely compensated by ~80%. Capacitive currents were elicited by brief 25 ms voltage steps of ±10 mV from a holding potential of −70 mV.

For current-clamp and voltage-clamp experiments involving *N-methyl*-D-glucamine (NMDG), a HEPES-buffered ACSF bath (150 mM

Table 1. Resting and active membrane properties of daytime and nighttime VIP⁺, NMS⁺, and GRP⁺ SCN neurons

		Firing rate (Hz)	R_{in} (GΩ)	V_m (mV)
Day	VIP⁺	3.1 ± 0.2[a]	2.2 ± 0.2[b]	−42.9 ± 0.8
		$n = 27$	$n = 27$	$n = 25$
	NMS⁺	3.4 ± 0.4[c]	2.7 ± 0.2[d]	−40.8 ± 1.1[e]
		$n = 19$	$n = 20$	$n = 22$
	GRP⁺	4.0 ± 0.5	3.1 ± 0.3[f]	−40.6 ± 0.5
		$n = 31$	$n = 18$	$n = 17$
Night	VIP⁺	2.0 ± 0.2[a]	1.4 ± 0.1[b]	−43.9 ± 1.1
		$n = 37$	$n = 22$	$n = 27$
	NMS⁺	1.4 ± 0.3[c]	1.9 ± 0.1[d]	−45.4 ± 0.8[e]
		$n = 13$	$n = 19$	$n = 19$
	GRP⁺	2.9 ± 0.3	2.0 ± 0.1[f]	−42.1 ± 0.6
		$n = 25$	$n = 15$	$n = 21$

Values are mean $\pm$ SEM; n = number of cells. R_{in}, input resistance; V_m, membrane potential.
[a-f] Values in daytime and nighttime VIP⁺(a,b), NMS⁺(c,d,e), and GRP⁺(f) SCN neurons are significantly different ([a,c,d,e,f] $p < 0.01$; [b] $p < 0.05$; Kolmogorov–Smirnov test).

NaCl, 3.5 mM KCl, 10 mM HEPES, 1.2 mM CaCl₂, 1 mM MgCl₂, 10 mM glucose, pH 7.3 with NaOH) was used (Jackson et al., 2004). For current-clamp recordings, spontaneous action potential firing was first recorded in HEPES-buffered standard ACSF bath solution, and TTX (1 μM) was added to the bath to silence the cell, followed by replacement of Na⁺ in the bath with NMDG⁺ via superfusion of an Na⁺-free, NMDG⁺-containing solution (150 mM NMDG-Cl, 3.5 mM KCl, 10 mM HEPES, 1.2 mM CaCl₂, 1 mM MgCl₂, 10 mM glucose, pH 7.3 with HCl) (Jackson et al., 2004). For voltage-clamp recordings, currents were recorded during slow voltage ramps (20 mV/s) from −100 to 20 mV in previously described conditions (Jackson et al., 2004): 1 μM TTX was first applied to the HEPES-buffered standard ACSF bath solution (to block voltage-gated Na⁺ currents), and then Na⁺ in the bath was replaced with NMDG⁺ by superfusion of Na⁺-free, NMDG⁺-containing solution. All chemicals and reagents were obtained from Sigma-Aldrich unless otherwise specified.

NALCN- and Kv12-encoded channel kinetic models and dynamic clamp recordings. A model of NALCN-encoded currents (I_{NALCN}) was formulated using the TTX-insensitive Na⁺ leak current data acquired from daytime WT SCN neurons. The NALCN-encoded current is calculated as follows: $I_{NALCN} = G_{NALCN}{}^{*}(V_m − E_{NALCN})$, where G_{NALCN} is a scalable conductance parameter for current magnitude and V_m is the membrane voltage. E_{NALCN} is the reversal potential for NALCN-encoded currents, set to −20 mV, which is the experimentally derived value for the TTX-insensitive Na⁺ leak currents. The previously described three-state Markov model of Kv12-encoded channel (I_{Kv12}) gating (Hermanstyne et al., 2023) was coded in MATLAB (The MathWorks). Dynamic clamp experiments were performed using the Cybercyte DC1 Dynamic Clamp System (Cytocybernetics) (Bett et al., 2013; Du et al., 2021), which consists of a 16 channel, 16 bit, 100 kS/s MCC PCle-DAS1602/16 board installed and configured in a Dell
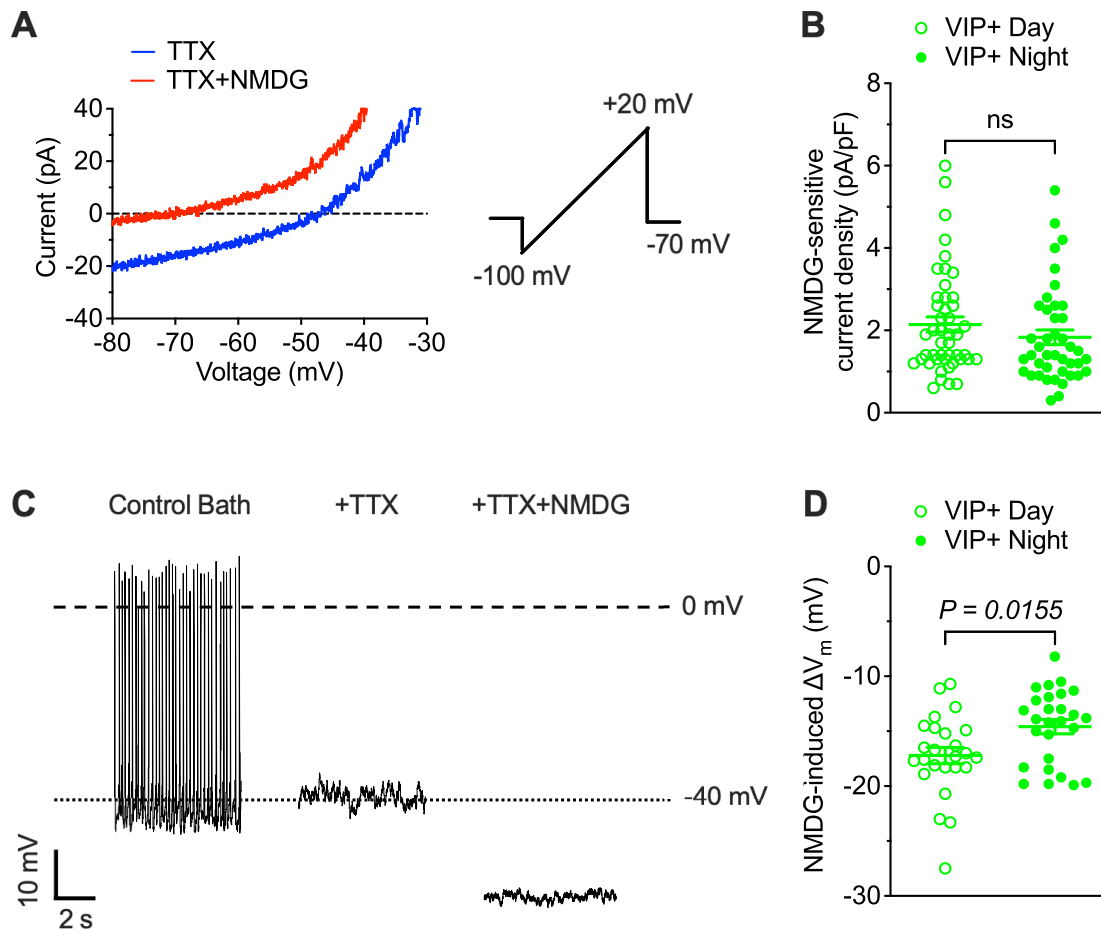
Figure 2. Differential effects of Na$^+$ leak currents on the membrane potentials of daytime and nighttime VIP$^+$ SCN neurons. **A**, Representative whole-cell currents recorded from a daytime VIP$^+$ SCN neuron during slow voltage ramps (20 mV/s) in the presence of 1 μM TTX (blue) and following NMDG$^+$ replacement of extracellular Na$^+$ (red). Addition of NMDG$^+$ decreases inward current amplitude. **B**, NMDG-sensitive Na$^+$ leak current densities measured in daytime (open circles, $n = 46$) and nighttime (filled circles, $n = 42$). VIP$^+$ SCN neurons are not significantly different. **C**, Representative whole-cell current-clamp recording from a daytime VIP$^+$ SCN neuron showing spontaneous action potential firing in control bath solution. The addition of 1 μM TTX eliminates firing but does not affect the resting membrane potential. The subsequent replacement of extracellular Na$^+$ with NMDG$^+$, however, hyperpolarizes the membrane potential. **D**, NMDG-induced changes in the membrane potentials of VIP$^+$ SCN neurons during the day (open circles, $n = 25$) and at night (filled circles, $n = 27$) are shown. Data are mean $\pm$ SEM; p values are also indicated. See Extended Data Figure 2-1 and Extended Data Table 2-1.

Precision 5820 Tower Workstation. The average loop time measured for the system was 22 μs.

Before experiments on SCN neurons, the I_{NALCN} and I_{Kv12} formulations were converted to Cybercyte channel definition files using the CyberSolver software (Cytocybernetics) and validated by applying the simulated currents in voltage-clamp mode to a Patch-1U model cell (Molecular Devices) in cell mode. The Cybercyte DC1 system allows current amplitudes to be scaled during dynamic clamp experiments to provide appropriate output size of the modeled currents. For I_{NALCN}, G_{NALCN} was set to a starting value of 0.2 nS to match the difference observed in I_{NaL} amplitudes of controls versus c*Nalcn*KO SCN neurons (see Fig. 5D), which equals 10 pA of inward current at -70 mV. For I_{Kv12}, G_{Kv12} was set to a starting value of 1 nS, that equals a peak current amplitude of 5 pA (Hermanstyne et al., 2023). In cases where I_{NALCN} was subtracted (by adding I_{NALCN} of opposite polarity) or I_{Kv12} was added by dynamic clamp in real time during whole-cell current-clamp recordings from daytime WT SCN neurons, G_{NALCN} or G_{Kv12} was scaled up/down from the starting values as necessary to achieve minimal current amplitudes required to reduce the spontaneous repetitive firing rates to the range of 1-2 Hz (typical of nighttime WT SCN neurons). For each cell, spontaneous repetitive firing was first recorded for 1 min. Modeled currents (I_{NALCN} or I_{Kv12}) were then subtracted or added separately, or in combination, in amplitudes determined as described above, and the resulting repetitive firing rates were measured.

Table 2. NMDG-sensitive Na$^+$ leak currents and NMDG-induced membrane potential changes in daytime and nighttime VIP$^+$, NMS$^+$, and GRP$^+$ SCN neurons

		I_{NaL} (pA/pF)	ΔV_m (mV)
Day	VIP$^+$	2.1 $\pm$ 0.2	-17.2 ± 0.7^a
		$n = 46$	$n = 25$
	NMS$^+$	1.9 $\pm$ 0.2	-18.2 ± 0.9^b
		$n = 38$	$n = 23$
	GRP$^+$	1.9 $\pm$ 0.2	-17.5 ± 0.8^c
		$n = 19$	$n = 20$
Night	VIP$^+$	1.8 $\pm$ 0.2	-14.6 ± 0.6^a
		$n = 42$	$n = 27$
	NMS$^+$	1.8 $\pm$ 0.2	-14.6 ± 0.8^b
		$n = 33$	$n = 19$
	GRP$^+$	1.7 $\pm$ 0.2	-13.9 ± 0.7^c
		$n = 23$	$n = 23$

Values are mean $\pm$ SEM; n = number of cells. I_{NaL}, NMDG-sensitive Na$^+$ leak current density; ΔV_m, NMDG-induced change in membrane potential.

[a-c]Mean ΔV_m values are different ($^{a,b}p < 0.05$; $^c p < 0.01$; Kolmogorov–Smirnov test) in daytime and nighttime VIP$^{+(a)}$, NMS$^{+(b)}$, and GRP$^{+(c)}$ SCN neurons. Mean daytime and nighttime I_{NaL} densities, in contrast, are similar in VIP$^+$, NMS$^+$, and GRP$^+$ SCN neurons.

Data analysis and statistics. Electrophysiological data were compiled and analyzed with ClampFit 11 (Molecular Devices), MATLAB (R2021a, The MathWorks), and Prism 9 (GraphPad) software. Cells with high series resistances (>25 Mohms) or low membrane resistances (<1 Gohm) were excluded. The firing rate of each cell was determined from the action potential firing detected in the initial 1 min recording period. The input resistance of each cell was calculated by measuring the steady-state voltage changes produced by ± 5 pA current injections from a holding potential of -70 mV. The membrane potentials (V_m) of spontaneously firing cells were estimated from phase plots (Bean, 2007) of spontaneous action potentials. For each cell, the first derivative of the membrane potential (dV/dt) was plotted as a function of the membrane potential (V), and V_m was estimated during the time window from ~20 ms following the peak of the action potential (to avoid including any portion of the afterhyperpolarization of the action potential) to the beginning of the next action potential as the average value of V for data points within dV/dt = $\pm$ 0.2 mV/ms. Whole-cell membrane capacitances (C_m) were determined from evoked capacitive currents, and were calculated by dividing the integrated capacitive transients by the voltage changes. The NMDG⁺-sensitive currents were obtained by subtraction of the inward ramp currents recorded after NMDG⁺ replacement for Na⁺ in the TTX-containing bath solution from the inward ramp currents recorded (in the same cell) in the TTX only-containing bath solution (i.e., before the replacement of the Na⁺ in the bath with NMDG⁺) (Jackson et al., 2004). The TTX-insensitive Na⁺ leak current was defined as the NMDG⁺-sensitive current at -70 mV. For each cell, Na⁺ leak current density (pA/pF) at -70 mV is reported. Statistical analyses were performed by Kolmogorov–Smirnov test for two-sample comparisons and by one-way ANOVA with Tukey's *post hoc* test for multiple comparisons. Statistical significance is set at $p < 0.05$. Normality and equal variance tests were performed for all statistical analyses. All average data are presented as mean $\pm$ SEM.
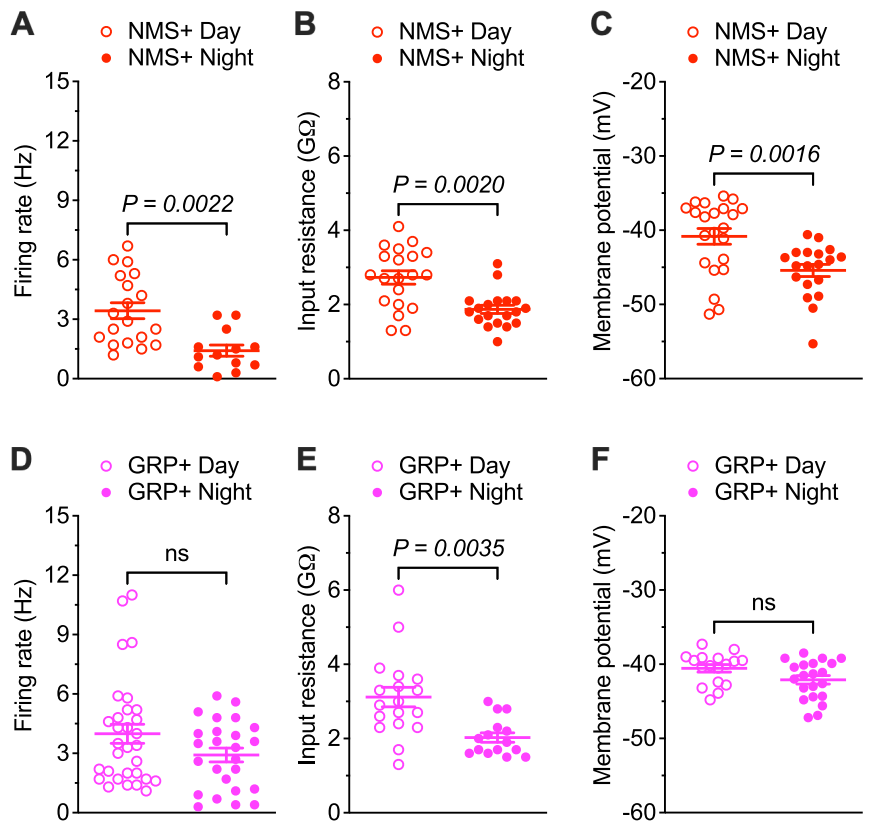

Figure 3. NMS⁺, but not GRP⁺, SCN neurons display day-night rhythms in spontaneous repetitive firing rates and membrane potentials. The spontaneous firing rates (*A*), input resistances (*B*), and membrane potentials (*C*) of individual NMS⁺ SCN neurons, measured in slices prepared during the day (red open circles, $n = 19$-22) or at night (red filled circles, $n = 13$-19) are plotted. The spontaneous firing rates (*D*), input resistances (*E*), and membrane potentials (*F*) measured in individual daytime (magenta open circles, $n = 17$-31) and nighttime (magenta filled circles, $n = 15$-25) GRP⁺ SCN neurons are plotted. Data are mean $\pm$ SEM; *p* values are also indicated.

Results

VIP-expressing SCN neurons display daily changes in spontaneous repetitive firing rates

To enable electrophysiological recordings from VIP-expressing (VIP⁺) SCN neurons, we used a VIP-EGFP mouse line that expresses EGFP in VIP cells (see Materials and Methods). The cell bodies of VIP⁺ (EGFP⁺) neurons were identified in the ventral region of the SCN (Fig. 1A), consistent with previous observations (Abrahamson and Moore, 2001). Whole-cell current-clamp recordings from VIP⁺ neurons in acute SCN slices prepared during the day (ZT5-ZT11) or at night (ZT17-ZT23) (see Materials and Methods) revealed that VIP⁺ SCN neurons are spontaneously active with higher mean $\pm$ SEM repetitive firing rates during the day than at night (Fig. 1B; Table 1). A day-night difference in mean $\pm$ SEM input resistance (R_{in}), with higher R_{in} during the day, was also observed in VIP⁺ SCN neurons (Fig. 1C; Table 1), whereas the mean $\pm$ SEM membrane potentials (V_m) of daytime and nighttime VIP⁺ SCN neurons were similar (Fig. 1D; Table 1). These

observations are consistent with the results of previous multi-electrode array and whole-cell patch-clamp recordings from VIP⁺ SCN neurons (Hermanstyne et al., 2016; Mazuski et al., 2018; Patton et al., 2020).

Differential effects of Na⁺ leak currents on daytime and nighttime VIP⁺ SCN neurons

To determine directly the role(s) of Na⁺ leak currents in controlling the membrane/firing properties of VIP⁺ SCN neurons, we conducted voltage-clamp experiments to isolate and measure the magnitudes of TTX-insensitive Na⁺ leak currents (I_{NaL}) using a previously described method (Jackson et al., 2004). Briefly, inward currents, evoked during slow voltage ramps (20 mV/s) from -100 to 20 mV, were first recorded in bath solution containing 1 μM TTX (to block voltage-gated Na⁺ currents) and again following the replacement of the Na⁺ in the bath solution with NMDG⁺ (see Materials and Methods). Representative ramp currents measured in a daytime VIP⁺ SCN neuron in the presence of TTX (blue) and TTX + NMDG⁺ (red) are presented in Figure 2A. Using this protocol on many daytime and nighttime VIP⁺ neurons revealed that I_{NaL} densities in VIP⁺ SCN neurons are small and quite variable (Fig. 2B; Table 2). Similar variability in I_{NaL} densities in (daytime and nighttime) VIP⁺ SCN neurons was evident across (daytime and nighttime) slices. Indeed, mean I_{NaL} densities determined in individual SCN are remarkably similar both during the day and at night (Extended Data Fig. 2-1A; Extended Data Table 2-1). In addition, these
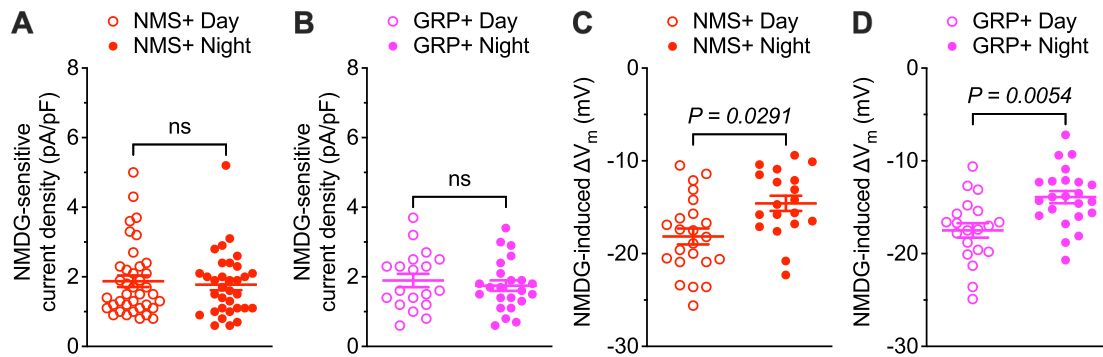
Figure 4. Differential effects of Na+ leak currents on the membrane potentials of daytime and nighttime NMS+ and GRP+ SCN neurons. NMDG-sensitive Na+ leak current densities, measured in (A) NMS+ (red) and (B) GRP+ (magenta) SCN neurons during the day (open circles; $n = 38$ for NMS+; $n = 19$ for GRP+) and at night (filled circles; $n = 33$ for NMS+; $n = 23$ for GRP+) are plotted. NMDG-induced changes in the membrane potentials of (C) NMS+ (red) and (D) GRP+ (magenta) SCN neurons during the day (open circles; $n = 23$ for NMS+; $n = 20$ for GRP+) and at night (filled circles; $n = 19$ for NMS+; $n = 23$ for GRP+) are plotted. Data are mean ± SEM; p values are also indicated. See Extended Data Figure 2-1 and Extended Data Table 2-1.

experiments revealed that mean ± SEM I_{NaL} densities in daytime and nighttime VIP+ SCN neurons are similar (Fig. 2B; Table 2).

To determine the contribution of Na+ leak currents to the membrane potentials of VIP+ SCN neurons, we obtained whole-cell current-clamp recordings from VIP+ neurons during the day and at night. After recording repetitive firing under control conditions, 1 μM TTX was added to the bath. Although repetitive firing was abolished with the addition of TTX as illustrated in Figure 2C, the resting membrane potential of the cell was not measurably affected (Fig. 2C). In contrast, when external Na+ was replaced with NMDG+, a large hyperpolarizing shift in the resting membrane potential was observed (Fig. 2C). Similar results were obtained in recordings from 25 daytime VIP+ SCN neurons with a mean ± SEM change in resting membrane potential of −17.2 ± 0.7 mV (Fig. 2D). Eliminating Na+ leak currents also resulted in hyperpolarizing shifts in the membrane potentials of nighttime VIP+ SCN neurons, although the magnitude of the shift, mean ± SEM of −14.6 ± 0.6 mV ($n = 27$), was less than observed in daytime VIP+ cells (Fig. 2D; Extended Data Fig. 2-1B; Table 2; Extended Data Table 2-1), revealing that Na+ leak currents have a greater influence on the resting membrane potentials of daytime, than nighttime, VIP+ SCN neurons.

Firing rates and membrane properties of NMS+ and GRP+ SCN neurons are distinct

Immunohistochemical and ISH studies have documented the differential expression of two other neuropeptides, NMS and GRP, in VIP+ SCN neurons (Romijn et al., 1998; Kawamoto et al., 2003; Lee et al., 2015). RNA sequencing studies have also revealed two molecularly distinct subtypes of VIP+ neurons in the SCN: one that coexpresses NMS (VIP+/NMS+) and the other that coexpresses GRP (VIP+/GRP+) (Todd et al., 2020; Wen et al., 2020). To explore the possibility that some of the variability in the daytime (and nighttime) repetitive firing rates (Fig. 1B), membrane properties (Fig. 1C,D), and I_{NaL} densities (Fig. 2B) observed in VIP+ SCN neurons reflects cellular heterogeneity, additional experiments were conducted on NMS-expressing (NMS+) and GRP-expressing (GRP+) neurons, which are nonoverlapping populations of VIP+ SCN neurons (Lee et al., 2015; Todd et al., 2020; Wen et al., 2020). To enable the identification of NMS+ and GRP+ neurons in SCN slices, we generated mouse lines expressing the red fluorescent protein, tdTomato, in NMS+ or GRP+ cells (NMS-tdTomato or GRP-tdTomato) by crossing NMS-iCre or GRP-Cre mice with Ai9 reporter mice

(see Materials and Methods). As previous reports demonstrated that NMS+ neurons are distributed through the ventral and dorsal regions of the SCN (Abrahamson and Moore, 2001; Morin et al., 2006; Lee et al., 2015), we specifically targeted tdTomato-expressing NMS+ neurons in the ventral region (where VIP+ neurons are located; see Fig. 1A).

Similar to VIP+ SCN neurons (Fig. 1B), whole-cell current-clamp recordings from NMS+ SCN neurons revealed robust daily variations in mean ± SEM spontaneous repetitive firing rates with higher firing rates during the day than at night (Fig. 3A; Table 1). In contrast, there was no significant day-night difference in the mean ± SEM spontaneous repetitive firing rates of GRP+ SCN neurons (Fig. 3D; Table 1). NMS+ SCN neurons also displayed a marked day-night difference (∼5 mV) in mean V_m with more hyperpolarized V_m at night than during the day (Fig. 3C; Table 1), whereas in GRP+ SCN neurons, V_m values were similar day and night (Fig. 3F; Table 1). Additional analyses revealed that the mean ± SEM repetitive firing rates of both daytime and nighttime GRP+ SCN neurons are comparable to those of daytime NMS+ SCN neurons ($p = 0.7864$ for daytime GRP+, $p = 0.8476$ for nighttime GRP+, one-way ANOVA) (Table 1). In addition, the mean ± SEM. V_m values determined for daytime and nighttime GRP+ SCN neurons are similar to daytime NMS+ SCN neurons ($p = 0.9948$ for daytime GRP+, $p = 0.6497$ for nighttime GRP+, one-way ANOVA) (Table 1). However, robust day-night oscillations of R_{in} (larger during the day than at night) were measured in both NMS+ and GRP+ SCN neurons (Fig. 3B, E; Table 1).

Differential effects of Na+ leak currents on NMS+ and GRP+ SCN neurons

Similar to the findings in VIP+ SCN neurons (Fig. 2B), voltage-clamp recordings revealed that I_{NaL} densities are highly variable in both daytime and nighttime NMS+ and GRP+ SCN neurons and, in addition, that mean ± SEM I_{NaL} densities are similar during the day and night in both cell types (Fig. 4A,B; Extended Data Fig. 2-1C,E; Table 2; Extended Data Table 2-1). Interestingly, however, eliminating Na+ leak currents resulted in larger hyperpolarizing shifts in the resting membrane potentials (∼4 mV difference) of both NMS+ and GRP+ SCN neurons during the day than at night (Fig. 4C,D; Extended Data Fig. 2-1D,F; Table 2; Extended Data Table 2-1). These observations, which are similar to the findings in VIP+ SCN neurons (Fig. 2D; Extended Data Fig. 2-1B), demonstrate that Na+ leak currents

also have a greater impact on the resting membrane potentials of daytime, than nighttime, NMS$^+$ and GRP$^+$ SCN neurons.

NALCN-encoded currents selectively regulate the excitability of daytime SCN neurons

To define the contribution of NALCN-encoded channels to I$_{NaL}$ in adult SCN neurons, we took advantage of the availability of *Nalcn*$^{fl/fl}$ mice in which exons 4 and 5 of *Nalcn* are flanked by loxP sites (Flourakis et al., 2015) to conditionally disrupt *Nalcn* in the adult SCN. Cre-dependent KO was produced by delivering an AAV expressing dTomato and Cre recombinase driven by a neuron-specific promoter (AAV5-hSyn-Cre-P2A-dTomato) directly to the SCN of adult *Nalcn*$^{fl/fl}$ mice (see Materials and Methods). Adult WT mice injected with the same virus were used as controls. Approximately 3-4 weeks after virus injections, acute SCN slices were prepared and dTomato$^+$ neurons in virus injected *Nalcn*$^{fl/fl}$ (c*Nalcn*KO) and WT mice (control) were targeted for whole-cell current-clamp recordings (Fig. 5A). Preliminary experiments revealed that the repetitive firing rates of virus-transduced and untransduced SCN neurons in slices prepared from virus-injected WT mice were similar (data not shown), demonstrating that the expression of dTomato and Cre recombinase does not affect the firing rates of WT SCN neurons. The mean $\pm$ SEM repetitive firing rate measured in neurons in daytime c*Nalcn*KO SCN slices, however, was substantially lower than the mean rate measured in virus-expressing WT controls (Fig. 5B; Table 3). In contrast, the mean $\pm$ SEM repetitive firing rate of nighttime c*Nalcn*KO SCN neurons was not significantly different from nighttime controls (Fig. 5B; Table 3). Disruption of *Nalcn* expression in SCN neurons, therefore, eliminates the day-night oscillations in the repetitive firing rates that are characteristic of WT SCN neurons (Fig. 5B; Table 3).

Consistent with the observed effects on mean repetitive firing rates, disruption of *Nalcn* expression in SCN neurons resulted in more hyperpolarized mean $\pm$ SEM. V_m during the day, but not at night (Fig. 5C; Table 3). As a result and in marked contrast with the robust day-night variations in mean $\pm$ SEM V_m observed in controls, c*Nalcn*KO SCN neurons displayed "nighttime-like" hyperpolarized V_m throughout the day-night cycle (Fig. 5C; Table 3). To confirm that the NALCN-encoded Na$^+$ leak currents were disrupted in the c*Nalcn*KO SCN neurons, we obtained whole-cell voltage-clamp recordings to quantify NMDG-sensitive Na$^+$ leak current amplitudes/densities (determined as described above and illustrated in Fig. 2A). The amplitudes/densities of I$_{NaL}$ in c*Nalcn*KO SCN neurons were ~50% of the I$_{NaL}$ amplitudes/densities measured in the controls for both daytime and nighttime SCN neurons (Fig. 5D; Table 3). The mean $\pm$ SEM R$_{in}$ measured in c*Nalcn*KO SCN neurons was also higher than in controls (Fig. 5E; Table 3), consistent with the elimination of subthreshold Na$^+$ currents. Together, these results demonstrate that conditional KO of *Nalcn* in adult SCN neurons reduced excitability during the day, but not at
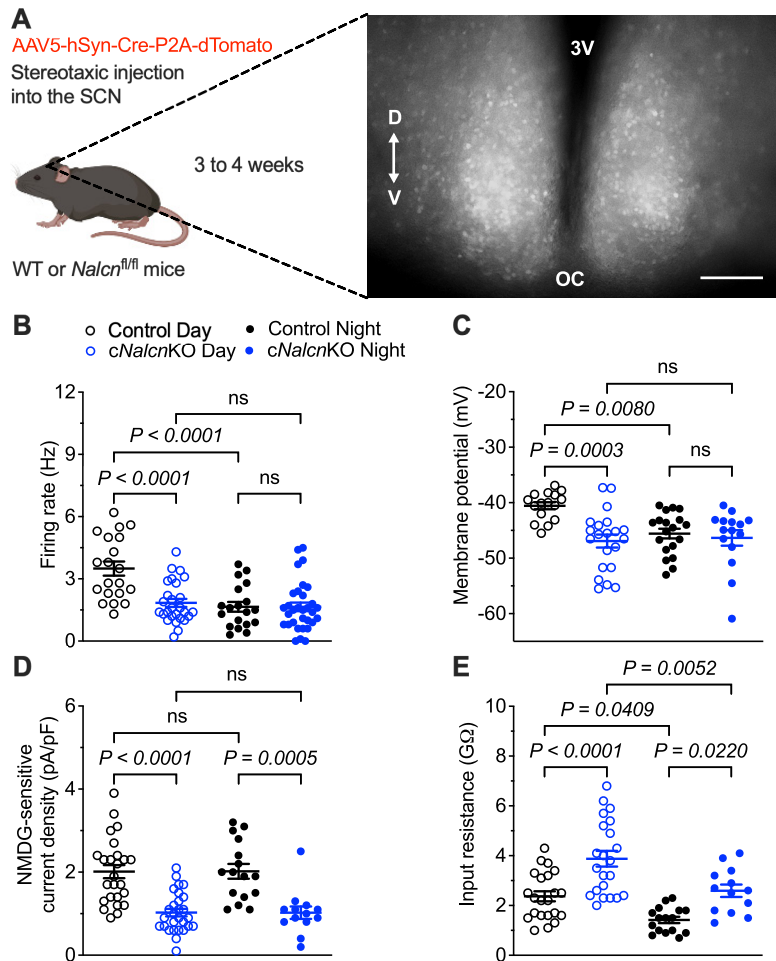

Figure 5. KO of *Nalcn* selectively decreases the excitability of daytime SCN neurons. *A*, *Nalcn* was conditionally disrupted following bilateral injections of the AAV5-hSyn-Cre-P2A-dTomato virus (see Materials and Methods) into the SCN of adult *Nalcn*$^{fl/fl}$ mice. Representative fluorescence image of an SCN slice prepared from an adult *Nalcn*$^{fl/fl}$ mouse 4 weeks after virus injection. Scale bar, 100 μm. V, Ventral; D, dorsal; 3V, third ventricle; OC, optic chiasm. The spontaneous firing rates (*B*), membrane potentials (*C*), NMDG-sensitive Na$^+$ leak current densities (*D*), and input resistances (*E*) of individual dTomato$^+$ control (black) and c*Nalcn*KO (blue) SCN neurons, measured in slices prepared during the day (open circles; n = 16-25 for controls; n = 21-28 for c*Nalcn*KO) or at night (filled circles; n = 16-19 for controls; n = 13-32 for c*Nalcn*KO) are plotted. *B–E*, Data are mean $\pm$ SEM; p values are also indicated.

Table 3. NMDG-sensitive Na$^+$ leak currents and firing properties of dTomato-positive control and c*Nalcn*KO SCN neurons during the day and at night

		Firing rate (Hz)	V_m (mV)	I$_{NaL}$ (pA/pF)	R$_{in}$ (GΩ)
Day	Control	3.5 $\pm$ 0.3[a,e]	−40.6 $\pm$ 0.6[b,f]	2.0 $\pm$ 0.2[c]	2.4 $\pm$ 0.2[d,g]
		n = 20	n = 16	n = 25	n = 22
	c*Nalcn*KO	1.8 $\pm$ 0.2[a]	−46.9 $\pm$ 1.2[b]	1.0 $\pm$ 0.1[c]	3.9 $\pm$ 0.3[d,j]
		n = 27	n = 21	n = 28	n = 22
Night	Control	1.7 $\pm$ 0.2[e]	−45.6 $\pm$ 0.9[f]	2.0 $\pm$ 0.2[h]	1.4 $\pm$ 0.1[g,i]
		n = 19	n = 19	n = 16	n = 16
	c*Nalcn*KO	1.7 $\pm$ 0.2	−46.4 $\pm$ 1.4	1.0 $\pm$ 0.1[h]	2.6 $\pm$ 0.2[i,j]
		n = 32	n = 15	n = 13	n = 13

Values are mean $\pm$ SEM; n = number of cells. V_m, membrane potential.
[a-d]Values in daytime dTomato$^+$ control and daytime dTomato$^+$ c*Nalcn*KO SCN neurons are significantly different ([a,c,d]$p < 0.0001$; [b]$p < 0.001$; one-way ANOVA with Tukey's *post hoc* test).
[e-g]Values in daytime and nighttime dTomato$^+$ control SCN neurons are significantly different ([e]$p < 0.0001$; [f]$p < 0.01$; [g]$p < 0.05$; one-way ANOVA with Tukey's *post hoc* test).
[h,i]Values in nighttime dTomato$^+$ control and nighttime dTomato$^+$ c*Nalcn*KO SCN neurons are significantly different ([h]$p < 0.001$; [i]$p < 0.05$; one-way ANOVA with Tukey's *post hoc* test).
[j]Values in daytime and nighttime dTomato$^+$ c*Nalcn*KO SCN neurons are significantly different ([j]$p < 0.01$; one-way ANOVA with Tukey's *post hoc* test).
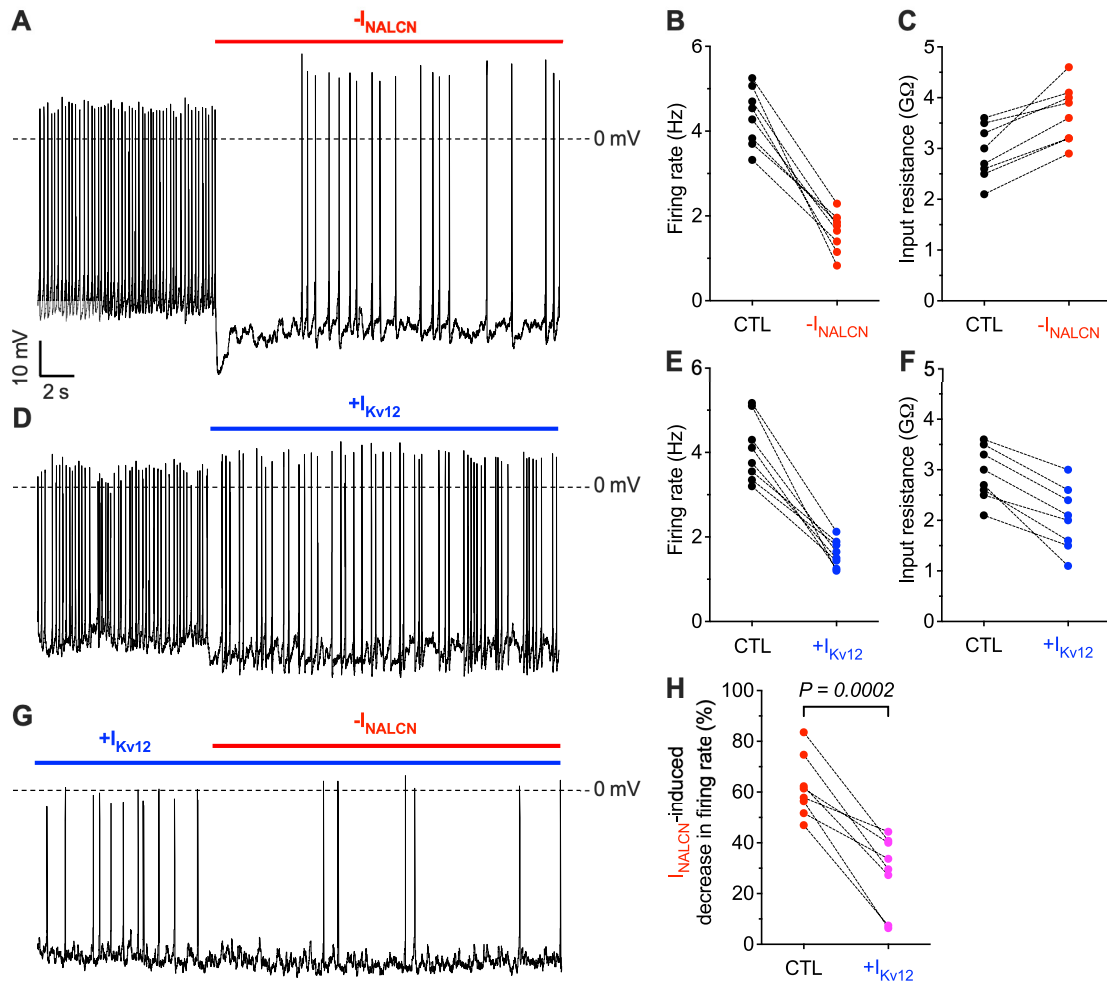
Figure 6. Effects of dynamic clamp-mediated manipulation of I$_{NALCN}$ and I$_{Kv12}$ on the spontaneous repetitive firing rates of WT SCN neurons. **A**, Representative whole-cell current-clamp recording from a daytime WT SCN neuron at baseline and with modeled I$_{NALCN}$ subtracted (red) via dynamic clamp. Spontaneous repetitive firing rates (**B**) and input resistances (**C**) of daytime WT SCN neurons at baseline (CTL) and with I$_{NALCN}$ subtracted (red). **D**, Representative whole-cell current-clamp recording from a daytime WT SCN neuron at baseline and with modeled I$_{Kv12}$ added (blue) via dynamic clamp. Spontaneous repetitive firing rates (**E**) and input resistances (**F**) of daytime WT SCN neurons at baseline (CTL) and with I$_{Kv12}$ added (blue). **G**, Representative whole-cell current-clamp recording from a daytime WT SCN neuron with modeled I$_{Kv12}$ added (blue) followed by subtraction of modeled I$_{NALCN}$ (red) via dynamic clamp. **H**, Percentage decrease in the firing rate induced by the subtraction of I$_{NALCN}$ in daytime WT SCN neurons at baseline (CTL, red) and with I$_{Kv12}$ added (magenta). Statistical significance was determined by paired Student's t test; p value is indicated. Data from the same cell are connected by dotted lines.

night, suggesting that NALCN-encoded Na$^+$ leak currents selectively modulate the excitability of daytime SCN neurons.

Dynamic clamp-mediated subtraction of NALCN-encoded Na$^+$ leak currents

To further explore the mechanism underlying the daytime-selective effects of NALCN-encoded Na$^+$ leak currents on the repetitive firing rates of SCN neurons (Fig. 5), we used the dynamic clamp technique (Prinz et al., 2004) to manipulate ionic currents electronically in real time during current-clamp recordings (see Materials and Methods). We formulated a leak current model for NALCN-encoded channels (I$_{NALCN}$) derived from the NMDG$^+$-sensitive leak currents measured in recordings from daytime WT SCN neurons (see Materials and Methods). Whole-cell current-clamp recordings were obtained from SCN neurons in acute slices prepared from adult WT mice during the day, and I$_{NALCN}$ was manipulated using dynamic clamp. As illustrated in the representative recording from a daytime WT SCN neuron shown in Figure 6A, subtraction of I$_{NALCN}$ (red) markedly decreased the

rate of repetitive firing and hyperpolarized V_m. Similar results were obtained in recordings from additional daytime WT SCN neurons (Fig. 6B). Subtraction of I$_{NALCN}$ led to increased R$_{in}$ in all cells (Fig. 6C). As expected, however, decreasing I$_{NALCN}$ is equivalent to increasing the R$_{in}$ which is opposite to what is observed experimentally in nighttime WT SCN neurons (Kuhlman and McMahon, 2004, 2006; Allen et al., 2017; Harvey et al., 2020; Hermanstyne et al., 2023).

To simulate the nighttime increase of subthreshold K$^+$ currents using dynamic clamp, we introduced I$_{Kv12}$, shown recently to regulate the day-night switch in the spontaneous firing rates and membrane properties of WT SCN neurons (Hermanstyne et al., 2023). Adding I$_{Kv12}$ in daytime WT SCN neurons markedly reduced repetitive firing rates (Fig. 6D,E) and decreased R$_{in}$ (Fig. 6F), effectively converting daytime neurons into nighttime-like SCN neurons. To test the hypothesis that the selective effect of NALCN-encoded Na$^+$ leak currents on the excitability of daytime SCN neurons depends on the robust night to day change in R$_{in}$ (i.e., higher R$_{in}$ during the day than at night) (Figs. 1, 3), we subtracted the same magnitude of I$_{NALCN}$ (red), in the same cell

as in Figure 6A–C, but in the presence of added I_{Kv12} (blue) (Fig. 6G). These experiments revealed that the subtraction of I_{NALCN} in the presence of increased I_{Kv12} resulted in only very modest changes in the repetitive firing rates of daytime WT SCN neurons (Fig. 6H) (i.e., recapitulating the observations in daytime and nighttime c*Nalcn*KO SCN neurons) (Fig. 5B). These results suggest that the effects of NALCN-encoded Na⁺ leak currents on the spontaneous repetitive firing rates are controlled by the K⁺ current-mediated differences in the R_{in} of daytime and nighttime SCN neurons.

Discussion

The results presented here demonstrate that the amplitudes of Na⁺ leak currents are similar in daytime and nighttime VIP⁺, NMS⁺, and GRP⁺ SCN neurons, but that these currents have a larger influence on membrane potentials during the day than at night (Figs. 1-4). Additional experiments revealed that the *in vivo* conditional KO of *Nalcn* in the SCN selectively decreased the repetitive firing rates of SCN neurons during the day, and eliminated the day-night difference in mean repetitive firing rates that is characteristics of WT SCN neurons (Fig. 5). Experiments using dynamic clamp to manipulate I_{NALCN} and I_{Kv12} demonstrated that the effects of NALCN-encoded Na⁺ leak currents on the repetitive firing rates of SCN neurons depend on the day-night differences in input resistances that result from changes in K⁺ currents (Fig. 6). Together, these results reveal a mechanism by which NALCN-encoded Na⁺ leak channels modulate daily rhythms in the rates of spontaneous action potential firing of SCN neurons as a consequence of rhythmic changes in subthreshold K⁺ currents. During the day, the impact of NALCN-encoded Na⁺ leak currents is amplified by higher input resistances driven by reductions in K⁺ currents, whereas, at night, the influence of NALCN-encoded Na⁺ leak currents of the same amplitude is attenuated because of lower input resistances, driven by increased K⁺ currents.

Na⁺ leak current amplitudes are similar in daytime and nighttime SCN neurons

Voltage-clamp recordings revealed that the mean ± SEM amplitudes/densities of the TTX-insensitive Na⁺ leak currents are similar in daytime and nighttime VIP⁺, NMS⁺, and GRP SCN neurons (Figs. 2B, 4A,B). These observations contrast with the findings in *Drosophila* DN1p clock neurons, which were shown to display a diurnal variation (higher during the day than at night) in the mean amplitude/density of the TTX-insensitive Na⁺ leak current (Flourakis et al., 2015). Eliminating the TTX-insensitive Na⁺ leak currents produced hyperpolarization of the resting membrane potentials in VIP⁺, NMS⁺, and GRP SCN neurons (Figs. 2D, 4C,D), indicating that Na⁺ leak currents are important for setting the V_m in SCN neurons.

The larger effect on membrane potentials observed in daytime, compared with nighttime, SCN neurons ($\sim$4 mV difference) (Figs. 2D, 4C,D), however, is similar to the findings for *Drosophila* DN1p neurons (Flourakis et al., 2015). Our results in SCN neurons, however, suggest such that the differential effects on V_m are driven by the robust daily changes in R_{in} (Figs. 1C, 3B, E, 6). In contrast, no significant diurnal rhythm was found in R_{in} of *Drosophila* DN1p neurons (Flourakis et al., 2015), suggesting that, in these (DN1p) neurons, the differential effects on V_m may simply reflect the day-night variations of Na⁺ leak current densities. Flourakis et al. (2015) also reported that the amplitudes/densities of TTX-insensitive Na⁺ leak currents are larger during

the subjective day than the subjective night (by $\sim$0.7 pA/pF) in recordings obtained from unidentified SCN neurons in acute slices prepared from 3-month-old WT mice (maintained in constant darkness for at least 3 weeks). This day-night difference, however, is likely difficult to resolve given the variability in the amplitudes/densities of the TTX-insensitive Na⁺ leak currents we observed during the day and at night in VIP⁺, NMS⁺, and GRP⁺ neurons (Figs. 2B, 4A,B). Additional experiments will be needed to determine whether there are specific cell populations in the SCN that display much more uniform TTX-insensitive Na⁺ leak current amplitudes/densities than observed in VIP⁺, NMS⁺, and GRP⁺ neurons localized in the ventral region of the SCN.

NALCN-encoded currents selectively modulate excitability of daytime SCN neurons

It has previously been shown that both germline KO and brain-specific KO of *Nalcn* in mice are neonatal lethal, demonstrating that *Nalcn* is crucial for survival in mammals (Lu et al., 2007; Yeh et al., 2017). To assess the role of *Nalcn* in adult SCN, therefore, we used an *in vivo* conditional KO strategy (Fig. 5A). Analysis of the properties of adult *Nalcn* KO SCN neurons revealed that disruption of *Nalcn* selectively decreased the repetitive firing rates of SCN neurons during the day but not at night (Fig. 5B). Our conditional *Nalcn* KO results resemble the findings in the SNr, in which AAV-mediated Cre-dependent KO of *Nalcn* reduced, but did not eliminate, the spontaneous firing rates of SNr neurons (Lutas et al., 2016).

Results from the c*Nalcn*KO SCN neurons also suggest that NALCN-encoded Na⁺ leak currents account for $\sim$50% of all NMDG-sensitive Na⁺ leak currents (Fig. 5D) and $\sim$40% of the NMDG-induced effects on membrane potentials (Fig. 2D, 4C,D, 5C). These findings suggest that there may be other TTX-resistant subthreshold Na⁺ currents expressed in SCN neurons and that these also play a role in controlling the repetitive firing rates of mature SCN neurons. Future studies, aimed at defining the possible functional roles of some potential candidate currents, such as HCN-, Nav1.8-, and/or Nav1.9-encoded inward currents (Colwell, 2011; Harvey et al., 2020), in the regulation of daily rhythms in the spontaneous repetitive firing rates of SCN neurons will certainly be of interest. Because disruption of *Nalcn* eliminates the day-night oscillations in the mean repetitive firing rates of SCN neurons (Fig. 5B), which synchronize and drive daily rhythms in physiology and behavior, it will also be of considerable interest to determine the impact of the *in vivo* conditional KO of *Nalcn* in the adult SCN on circadian behavioral rhythms.

References

Abrahamson EE, Moore RY (2001) Suprachiasmatic nucleus in the mouse: retinal innervation, intrinsic organization and efferent projections. Brain Res 916:172–191.

Allen CN, Nitabach MN, Colwell CS (2017) Membrane currents, gene expression, and circadian clocks. Cold Spring Harb Perspect Biol 9: a027714.

Bean BP (2007) The action potential in mammalian central neurons. Nat Rev Neurosci 8:451–465.

Bett GC, Kaplan AD, Lis A, Cimato TR, Tzanakakis ES, Zhou Q, Morales MJ, Rasmusson RL (2013) Electronic 'expression' of the inward rectifier in cardiocytes derived from human-induced pluripotent stem cells. Heart Rhythm 10:1903–1910.

Collins B, Pierre-Ferrer S, Muheim C, Lukacsovich D, Cai Y, Spinnler A, Herrera CG, Wen S, Winterer J, Belle MD, Piggins HD, Hastings M, Loudon A, Yan J, Foldy C, Adamantidis A, Brown SA (2020) Circadian

VIPergic neurons of the suprachiasmatic nuclei sculpt the sleep-wake cycle. Neuron 108:486–499.e5.

Colwell CS (2011) Linking neural activity and molecular oscillations in the SCN. Nat Rev Neurosci 12:553–569.

de Jeu M, Hermes M, Pennartz C (1998) Circadian modulation of membrane properties in slices of rat suprachiasmatic nucleus. Neuroreport 9:3725–3729.

Du C, Rasmusson RL, Bett GC, Franks B, Zhang H, Hancox JC (2021) Investigation of the effects of the short QT syndrome D172N Kir2.1 mutation on ventricular action potential profile using dynamic clamp. Front Pharmacol 12:794620.

Flourakis M, Kula-Eversole E, Hutchison AL, Han TH, Aranda K, Moose DL, White KP, Dinner AR, Lear BC, Ren D, Diekman CO, Raman IM, Allada R (2015) A conserved bicycle model for circadian clock control of membrane excitability. Cell 162:836–848.

Granados-Fuentes D, Norris AJ, Carrasquillo Y, Nerbonne JM, Herzog ED (2012) I(A) channels encoded by Kv1.4 and Kv4.2 regulate neuronal firing in the suprachiasmatic nucleus and circadian rhythms in locomotor activity. J Neurosci 32:10045–10052.

Granados-Fuentes D, Hermanstyne TO, Carrasquillo Y, Nerbonne JM, Herzog ED (2015) IA channels encoded by Kv1.4 and Kv4.2 regulate circadian period of PER2 expression in the suprachiasmatic nucleus. J Biol Rhythms 30:396–407.

Green DJ, Gillette R (1982) Circadian rhythm of firing rate recorded from single cells in the rat suprachiasmatic brain slice. Brain Res 245:198–200.

Harvey JR, Plante AE, Meredith AL (2020) Ion channels controlling circadian rhythms in suprachiasmatic nucleus excitability. Physiol Rev 100:1415–1454.

Hastings MH, Maywood ES, Brancaccio M (2018) Generation of circadian rhythms in the suprachiasmatic nucleus. Nat Rev Neurosci 19:453–469.

Hastings MH, Maywood ES, Brancaccio M (2019) The mammalian circadian timing system and the suprachiasmatic nucleus as its pacemaker. Biology (Basel) 8:13.

Hermanstyne TO, Simms CL, Carrasquillo Y, Herzog ED, Nerbonne JM (2016) Distinct firing properties of vasoactive intestinal peptide-expressing neurons in the suprachiasmatic nucleus. J Biol Rhythms 31:57–67.

Hermanstyne TO, Granados-Fuentes D, Mellor RL, Herzog ED, Nerbonne JM (2017) Acute knockdown of Kv4.1 regulates repetitive firing rates and clock gene expression in the suprachiasmatic nucleus and daily rhythms in locomotor behavior. eNeuro 4:ENEURO.0377-16.2017.

Hermanstyne TO, Yang ND, Granados-Fuentes D, Li X, Mellor RL, Jegla T, Herzog ED, Nerbonne JM (2023) Kv12-encoded K$^+$ channels drive the day-night switch in the repetitive firing rates of SCN neurons. J Gen Physiol, in press.

Herzog ED, Hermanstyne T, Smyllie NJ, Hastings MH (2017) Regulating the suprachiasmatic nucleus (SCN) circadian clockwork: interplay between cell-autonomous and circuit-level mechanisms. Cold Spring Harb Perspect Biol 9:a027706.

Inouye ST, Kawamura H (1979) Persistence of circadian rhythmicity in a mammalian hypothalamic 'island' containing the suprachiasmatic nucleus. Proc Natl Acad Sci USA 76:5962–5966.

Itri JN, Michel S, Vansteensel MJ, Meijer JH, Colwell CS (2005) Fast delayed rectifier potassium current is required for circadian neural activity. Nat Neurosci 8:650–656.

Itri JN, Vosko AM, Schroeder A, Dragich JM, Michel S, Colwell CS (2010) Circadian regulation of a-type potassium currents in the suprachiasmatic nucleus. J Neurophysiol 103:632–640.

Jackson AC, Yao GL, Bean BP (2004) Mechanism of spontaneous firing in dorsomedial suprachiasmatic nucleus neurons. J Neurosci 24:7985–7998.

Jiang ZG, Yang Y, Liu ZP, Allen CN (1997) Membrane properties and synaptic inputs of suprachiasmatic nucleus neurons in rat brain slices. J Physiol 499:141–159.

Kawamoto K, Nagano M, Kanda F, Chihara K, Shigeyoshi Y, Okamura H (2003) Two types of VIP neuronal components in rat suprachiasmatic nucleus. J Neurosci Res 74:852–857.

Kent J, Meredith AL (2008) BK channels regulate spontaneous action potential rhythmicity in the suprachiasmatic nucleus. PLoS One 3:e3884.

Kononenko NI, Dudek FE (2004) Mechanism of irregular firing of suprachiasmatic nucleus neurons in rat hypothalamic slices. J Neurophysiol 91:267–273.

Kudo T, Loh DH, Kuljis D, Constance C, Colwell CS (2011) Fast delayed rectifier potassium current: critical for input and output of the circadian system. J Neurosci 31:2746–2755.

Kuhlman SJ, McMahon DG (2004) Rhythmic regulation of membrane potential and potassium current persists in SCN neurons in the absence of environmental input. Eur J Neurosci 20:1113–1117.

Kuhlman SJ, McMahon DG (2006) Encoding the ins and outs of circadian pacemaking. J Biol Rhythms 21:470–481.

Lee IT, Chang AS, Manandhar M, Shan Y, Fan J, Izumo M, Ikeda Y, Motoike T, Dixon S, Seinfeld JE, Takahashi JS, Yanagisawa M (2015) Neuromedin s-producing neurons act as essential pacemakers in the suprachiasmatic nucleus to couple clock neurons and dictate circadian rhythms. Neuron 85:1086–1102.

Lu B, Su Y, Das S, Liu J, Xia J, Ren D (2007) The neuronal channel NALCN contributes resting sodium permeability and is required for normal respiratory rhythm. Cell 129:371–383.

Lutas A, Lahmann C, Soumillon M, Yellen G (2016) The leak channel NALCN controls tonic firing and glycolytic sensitivity of substantia nigra pars reticulata neurons. Elife 5:e15271.

Madisen L, Zwingman TA, Sunkin SM, Oh SW, Zariwala HA, Gu H, Ng LL, Palmiter RD, Hawrylycz MJ, Jones AR, Lein ES, Zeng H (2010) A robust and high-throughput Cre reporting and characterization system for the whole mouse brain. Nat Neurosci 13:133–140.

Mazuski C, Abel JH, Chen SP, Hermanstyne TO, Jones JR, Simon T, Doyle FJ, Herzog ED (2018) Entrainment of circadian rhythms depends on firing rates and neuropeptide release of VIP SCN neurons. Neuron 99:555–563.e5.

Meredith AL, Wiler SW, Miller BH, Takahashi JS, Fodor AA, Ruby NF, Aldrich RW (2006) BK calcium-activated potassium channels regulate circadian behavioral rhythms and pacemaker output. Nat Neurosci 9:1041–1049.

Morin LP, Shivers KY, Blanchard JH, Muscat L (2006) Complex organization of mouse and rat suprachiasmatic nucleus. Neuroscience 137:1285–1297.

Patton AP, Edwards MD, Smyllie NJ, Hamnett R, Chesham JE, Brancaccio M, Maywood ES, Hastings MH (2020) The VIP-VPAC2 neuropeptidergic axis is a cellular pacemaking hub of the suprachiasmatic nucleus circadian circuit. Nat Commun 11:3394.

Pennartz CM, de Jeu MT, Geurtsen AM, Sluiter AA, Hermes ML (1998) Electrophysiological and morphological heterogeneity of neurons in slices of rat suprachiasmatic nucleus. J Physiol 506:775–793.

Pennartz CM, de Jeu MT, Bos NP, Schaap J, Geurtsen AM (2002) Diurnal modulation of pacemaker potentials and calcium current in the mammalian circadian clock. Nature 416:286–290.

Pitts GR, Ohta H, McMahon DG (2006) Daily rhythmicity of large-conductance Ca^{2+}-activated K$^+$ currents in suprachiasmatic nucleus neurons. Brain Res 1071:54–62.

Prinz AA, Abbott LF, Marder E (2004) The dynamic clamp comes of age. Trends Neurosci 27:218–224.

Romijn HJ, Sluiter AA, Wortel J, Van Uum JF, Buijs RM (1998) Immunocytochemical evidence for a diurnal rhythm of neurons showing colocalization of VIP with GRP in the rat suprachiasmatic nucleus. J Comp Neurol 391:397–405.

Todd WD, Venner A, Anaclet C, Broadhurst RY, De Luca R, Bandaru SS, Issokson L, Hablitz LM, Cravetchi O, Arrigoni E, Campbell JN, Allen CN, Olson DP, Fuller PM (2020) Suprachiasmatic VIP neurons are required for normal circadian rhythmicity and comprised of molecularly distinct subpopulations. Nat Commun 11:4410.

Welsh DK, Logothetis DE, Meister M, Reppert SM (1995) Individual neurons dissociated from rat suprachiasmatic nucleus express independently phased circadian firing rhythms. Neuron 14:697–706.

Wen S, Ma D, Zhao M, Xie L, Wu Q, Gou L, Zhu C, Fan Y, Wang H, Yan J (2020) Spatiotemporal single-cell analysis of gene expression in the mouse suprachiasmatic nucleus. Nat Neurosci 23:456–467.

Whitt JP, Montgomery JR, Meredith AL (2016) BK channel inactivation gates daytime excitability in the circadian clock. Nat Commun 7:10837.

Yeh SY, Huang WH, Wang W, Ward CS, Chao ES, Wu Z, Tang B, Tang J, Sun JJ, van der Heijden ME, Gray PA, Xue M, Ray RS, Ren D, Zoghbi HY (2017) Respiratory network stability and modulatory response to substance P require Nalcn. Neuron 94:294–303.e4.

Yu YQ, Barry DM, Hao Y, Liu XT, Chen ZF (2017) Molecular and neural basis of contagious itch behavior in mice. Science 355:1072–1076.